Structure of Solvated $Fe(CO)_5$: A Concerted XAFS, FTIR, and DFT Study of Solvation in Fluorinated Arenes

Taewoo Lee, Emma Welch, and Christoph G. Rose-Petruck*

Department of Chemistry, Brown University, Box H, Providence, Rhode Island 02912

Received: June 9, 2004; In Final Form: October 15, 2004

The structures of iron pentacarbonyl, $Fe(CO)_5$, solvated in benzene and its fluorinated derivatives have been investigated by X-ray absorption fine structure (XAFS) spectroscopy and infrared (IR) spectroscopy as well as density functional theory (DFT) calculations. As discussed previously (Jiang, Y.; Lee, T.; Rose-Petruck, C. *J. Phys. Chem. A* **2003**, *107*, 7524−7538), 60−90% of iron pentacarbonyl (IPC) molecules are distorted to C_{2v} symmetry in aromatic solvents at room temperature. Typically one solvent molecule interacts with the iron atom of IPC trans to the apical CO ligand forming an IPC···solvent complex. In substituted benzene several IPC···solvent complex conformations coexist. The relative conformer populations were determined by IR spectroscopy. These populations were subsequently used to determine the equilibrium structures of each conformer through the analysis of XAFS spectra in combination with DFT structural data for the IPC···solvent complexes.

1. Introduction

Transition metal carbonyls are of great importance in many areas of chemistry such as organometallic synthesis, catalysts, biological processes, and materials chemistry.[2−7] The mechanisms of their chemical reactions have been studied in the gas and liquid phases by static and time-resolved methods.[8−24] The photoinduced reaction mechanisms of $Fe(CO)_5$ and its ultrafast reaction dynamics have been investigated extensively in recent years with particular attention to possible singlet-to-triplet intersystem crossing during ligand dissociation and substitution processes.[16,19,20]

These studies assumed a D_{3h} ground-state symmetry of $Fe(CO)_5$, which is correct in the gas phase. In alcohols, aromatic solvents, and many other solvents, however, interactions between iron pentacarbonyl (IPC) and a single solvent molecule lead to the formation of an IPC−solvent (IPC−S) complex, thereby substantially distorting the geometry of IPC.[1] This can have significant mechanistic consequences for ligand substitution reactions, as the metal center is directly exposed to a single solvent molecule. Here we investigate the influence of the fluorination of benzene on the IPC···solvent (IPC···S) complex formation.

The theoretically most stable geometry for $Fe(CO)_5$ and other d^6 systems is D_{3h},[25,26] which has been confirmed by X-ray[27] and electron diffraction studies.[28−30] $Fe(CO)_5$ can undergo Berry pseudorotation[31] via a C_{4v} transition state. Its energy was determined to be between 0.6 [25,32] and 2.3 kcal/mol [33] higher than that of the D_{3h} geometry. The lifetime for each configuration in liquid IPC at 250 K has been estimated to be between 10 and 90 ps with a 1 kcal/mol energy barrier for pseudorotation in solution.[34] While solvated iron pentacarbonyl is, of course, surrounded by many solvent molecules, we recently determined that the specific interaction with a single molecule stabilizes the complex in the vicinity of the transition state.[1] As a consequence, solvated iron pentacarbonyl does not exist primarily in its gas-phase geometry. Instead, a conformer distribution is established that spans all symmetries between D_{3h} and C_{4v}. The structural deformations are directly related to the specific solute−solvent interaction strength and distance. Several other systems that exhibit D_{3h} as well as C_{4v} conformation are known.[35−39] To date, only a few studies have investigated these conformers theoretically or at interfaces.[40−42] We showed previously[1] that at thermal equilibrium $Fe(CO)_5(C_{2v})$ is the dominant conformer in aromatic solvents with a solvent molecule directly interacting with the iron center. In the resulting IPC···solvent (IPC···S) complex, the solvent molecule is located trans to the apical ligand of $Fe(CO)_5(C_{2v})$. Such a complex exhibits specific Fourier transform infrared (FTIR) active bands that are nonexistent in $Fe(CO)_5(D_{3h})$. For the studies reported here, we applied IR measurements in combination with X-ray absorption fine structure (XAFS) measurements and density functional theory (DFT) calculations for the determination of the relative conformer concentrations and structures of the IPC···S complex in benzene and its fluorinated derivatives. Benzene interacts with the iron center through one of its aryl hydrogens.[1] Here we will show that fluorinated benzenes interact in a similar geometry through either a hydrogen or a fluorine. We transcend our previous methods[1] to the analysis of solvent systems in which several IR-active conformers are simultaneously present.

The concerted application of IR and XAFS spectroscopies is beneficial. IR absorption spectra are caused by transitions into symmetry-dependent vibrational normal modes of the molecules. As discussed above, the IPC···S interactions change the symmetry of IPC, yielding various simultaneously existing IPC conformers. IR spectra can be used for the determination of the conformer populations. The normal-mode frequencies are, of course, parametrized by the intramolecular bond distances, but the spectra do not permit the measurement of these distances. Conversely, XAFS spectra measure these distances rather directly but, for the complexes investigated here, are not sensitive to their symmetries. The XAFS spectra are parametrized by the amplitude of the normal-mode vibrations,

* Corresponding author. Telephone: (401) 863-1533. Fax: (401) 863-2594. E-mail: Christoph_Rose-Petruck@brown.edu.

10.1021/jp047504u CCC: $27.50
Published on Web 12/02/2004

expressed by Debye−Waller factors in the XAFS equations.[43−45] Thus, both IR and XAFS spectra provide conjugate information that permits the measurement of the symmetry as well as bond lengths within IPC and its associated solvent molecule. This paper is divided into two main sections. The first presents the measurement of the conformer distributions of IPC in cyclohexane (CH), benzene (Bz), fluorobenzene (FBz), pentafluorobenzene (PFBz), and hexafluorobenzene (HFBz). In the second section, knowledge of the conformer populations is important for the subsequent analysis of the measured XAFS spectra because they are superpositions of XAFS spectra for each conformer. The analysis of the experimental data was aided by DFT calculations.

DFT Calculations. We carried out density functional theory (DFT) calculations of the structures of all conformers of the IPC···S complexes for all investigated solvent systems. The structures provided the initial estimate for the structural data used in the analysis process of the XAFS spectra. Additionally, using the calculated structures, we calculated the integrated IR absorption coefficients for the ν_1, ν_6, and ν_{10} vibrational modes that were used in the IR data analysis. All calculations of the IPC···S complex were carried out using Jaguar.[46] A B3LYP model with LACVP** basis set was used in all DFT calculations. None of these calculations found evidence that IPC interacts directly with the π orbitals of the aromatic ring. Instead, the most stable complexes are formed by the interaction between the iron atom and one aryl hydrogen or one aryl fluorine of the aromatic solvent. Thus three basic conformers of the IPC can exist simultaneously in solution: IPC···S_{aryl-H}, IPC···S_{aryl-F}, and undistorted IPC with D_{3h} symmetry. The interaction through the aryl-H exhibits several features of a hydrogen bond. The calculated bond lengths of the interacting C−H group increases by about 1.5 pm as the distance between IPC and the aryl hydrogen decreases. Simultaneously, electron density shifts from the metal center to the aryl hydrogen and the Fe−H−C bond path straightens. The total energies of the aryl-H and aryl-F conformers of the IPC···S complexes were minimized under the constraints of various solvent−iron distances ranging from 330 to 225 pm. As an example, the IPC···HFBz structure at 260 pm molecular separation is shown in Figure 1. Structures for IPC···Bz have been published earlier.[1]

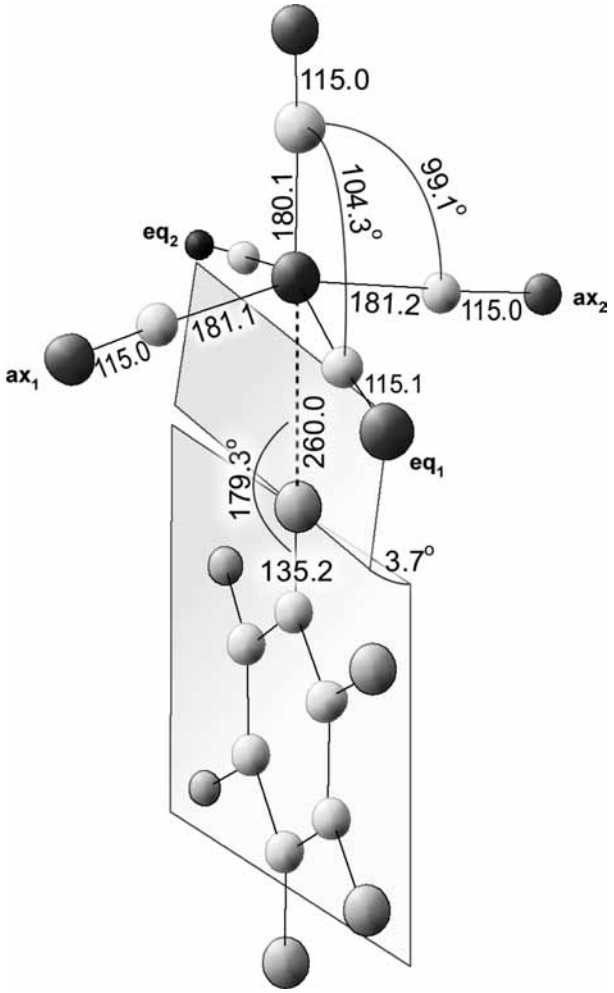

Figure 1. Representative IPC···HFBz structure at average solute−solvent distances. All dimensions are in picometers.

2. Conformer Populations

Solvated $Fe(CO)_5$ has been spectroscopically investigated for decades, and the CO stretching modes of $Fe(CO)_5$ with D_{3h} symmetry are well-known.[47−61] In principle, near-infrared spectra permit the determination of molecular symmetries. For instance, transition metal carbonyl complexes with D_{3h} symmetry exhibit two prominent peaks that correspond to the IR-active CO stretching modes $\nu_{10}(E')$ and $\nu_6(A_2'')$. For solvated IPC they appear between 1967 and 2034 cm^{-1}. In general, the peaks are red shifted relative to the gas-phase peaks and, depending on the solvent, are broadened. Complex deformations leading to C_{2v} or C_{4v} structures give rise to peaks in the same spectral region, which makes the determination of molecular geometries based solely on these peaks very difficult. In contrast, at higher energies of about 2115 cm^{-1}, the ν_1 normal mode is Raman active but not IR active for IPC in D_{3h} symmetry. This peak becomes IR active for $Fe(CO)_5(C_{2v},C_{4v})$ due to the reduced conformer symmetry, an effect observed in many pentacoordinated mixed-ligand[58,62−65] or chemisorbed[42] complexes. Since the complex deformation is a prerequisite for the IR activity of the ν_1 mode, we used its peak area as a measure of the population of deformed IPC. The measured peak areas and positions of the ν_1, ν_6, and ν_{10} modes are listed in Table 1. When analyzing this area in various solutions, the respective dielectric constants must be considered. We therefore always normalized ν_1 peak areas by the sum of the peak areas of $\nu_{10}(E')$ and $\nu_6(A_2'')$ before further processing. Measuring the area at various temperatures yields the Gibbs free energy for the deformation from D_{3h} to C_{2v} or C_{4v} symmetries. The analysis relies on the fact that only two kinds of conformers have to be considered with one of them, the D_{3h} conformer, not contributing to the IR spectrum at all. Of course, a distribution of C_{2v} conformers exists in solution and the analysis does not permit the determination of the exact geometries. However, IR data analysis in combination with DFT structure calculations can yield estimates for the complex structures. Details have been discussed in an earlier publication.[1] Here the IR data analysis procedure is extended to the treatment of systems in which several different types of conformers are present simultaneously. The procedure relies on the existence of compounds that have common conformer structures, such as Bz, FBz, PFBz, and HFBz. Their experimental IR spectra are analyzed simultaneously. As discussed above, the spectral analysis of Bz and HFBz only needs to consider D_{3h} and non-D_{3h} (C_{2v}) conformers. The C_{2v} structures are characterized by the interaction of the iron center with one aryl-H or one aryl-F for Bz and HFBz, respectively. In contrast, the spectra of FBz and PFBz include contributions from aryl-H and aryl-F conformers. This super-

TABLE 1: IR Peak Areas and Positions

IPC−S structure		M_1[a]	M_2+M_3[b]	M_4[c]	$M_1/(M_2+M_3)$	$M_1+M_2+M_3$	$M_4/(M_1+M_2+M_3)$
CH	freq (cm^{-1})	1998.94	2021.76	2113.27			
	integrated abs coeff (km/mol)	2365.31	1362.48	0.07	1.74	3727.79	0.002%
Bz	freq (cm^{-1})	1993.95	2019.97	2113.27			
	integrated abs coeff (km/mol)	2254.88	1631.80	2.72	1.38	3886.68	0.070%
FBz	freq (cm^{-1})	1994.85	2021.19	2114.03			
	integrated abs coeff (km/mol)	2382.07	1616.39	3.78	1.47	3998.46	0.095%
PFBz	freq (cm^{-1})	1997.76	2024.02	2115.59			
	integrated abs coeff (km/mol)	2625.41	1779.82	5.72	1.48	4405.23	0.130%
HFBz	freq (cm^{-1})	2002.59	2022.59	2115.64			
	integrated abs coeff (km/mol)	3284.74	1613.68	11.71	2.04	4898.42	0.239%

[a] Peak corresponds to $\nu_{10}(D_{3h}) + \nu_4(C_{2v}$ and $C_{4v})$. [b] Peak corresponds to $\nu_2(D_{3h}) + \nu_6(D_{3h})$ and $\nu_3(C_{2v}$ and $C_{4v}) + \nu_2(C_{2v}$ and $C_{4v})$. [c] Peak corresponds to $\nu_1(D_{3h}$, C_{2v}, and $C_{4v})$.

position is expressed for FBz in eq 1. An equivalent equation holds for PFBz.

$$\frac{A_{\nu_1}^{\exp}(\mathrm{FBz})}{A_{\nu_{6,10}}^{\exp}(\mathrm{FBz})} = \alpha\frac{A_{\nu_1}(\mathrm{FBz}_{\mathrm{aryl-F}})}{A_{\nu_{6,10}}(\mathrm{FBz}_{\mathrm{aryl-F}})} + \beta\frac{A_{\nu_1}(\mathrm{FBz}_{\mathrm{aryl-H}})}{A_{\nu_{6,10}}(\mathrm{FBz}_{\mathrm{aryl-H}})} + \chi\frac{A_{\nu_1}^{\mathrm{theo}}(D_{3h})}{A_{\nu_{6,10}}^{\exp}(D_{3h})} \quad (1)$$

In eq 1, $A_{\nu_1}^{\mathrm{theo}}(D_{3h}) \cong 0$. The constants α, β, and χ are the relative populations of each conformer, the sum of which has to be unity; thus

$$\alpha + \beta + \chi = 100\% \quad (2)$$

Jiang et al.[1] determined the equilibrium constant for the $D_{3h}-C_{2v}$ transformation for Bz, which defines the relation between β and χ.

$$\frac{\beta}{61.6\%} = \frac{\chi}{38.4\%} \leftrightarrow \chi = 0.62\beta \quad (3)$$

In FBz and PFBz it is impossible to measure each conformer's contribution because the conformers cannot be experimentally isolated. This seems to suggest that the aryl-H and aryl-F terms in eq 1 cannot be evaluated. However, our calculated infrared absorption coefficients are nearly equal for all aryl-H conformers calculated at identical aryl-H−Fe distances. Similarly, the ν_1 peak areas for aryl-F conformers of fluorinated benzene derivatives are nearly equal at identical aryl-F−Fe distances. Consequently, we assume that the normalized ν_1 peak area for the aryl-H conformer is identical to that of benzene, i.e.

$$\frac{A_{\nu_1}(\mathrm{FBz}_{\mathrm{aryl-F}})}{A_{\nu_{6,10}}(\mathrm{FBz}_{\mathrm{aryl-F}})} = \frac{A_{\nu_1}^{\exp}(\mathrm{HFBz})}{A_{\nu_{6,10}}^{\exp}(\mathrm{HFBz})} \quad (4)$$

and

$$\frac{A_{\nu_1}(\mathrm{FBz}_{\mathrm{aryl-H}})}{A_{\nu_{6,10}}(\mathrm{FBz}_{\mathrm{aryl-H}})} = \frac{A_{\nu_1}^{\exp}(\mathrm{Bz})}{A_{\nu_{6,10}}^{\exp}(\mathrm{Bz})} \quad (5)$$

Combining eqs 1−5 yields the conformer populations for the aryl-F conformer

$$\alpha = \frac{1.62A}{1.62 - B} - \frac{B}{1.62 - B} \quad (6)$$

with

$$A = \frac{A_{\nu_1}^{\exp}(\mathrm{FBz})}{A_{\nu_{6,10}}^{\exp}(\mathrm{FBz})} \Big/ \frac{A_{\nu_1}^{\exp}(\mathrm{HFBz})}{A_{\nu_{6,10}}^{\exp}(\mathrm{HFBz})} \quad \text{and}$$

$$B = \frac{A_{\nu_1}^{\exp}(\mathrm{Bz})}{A_{\nu_{6,10}}^{\exp}(\mathrm{Bz})} \Big/ \frac{A_{\nu_1}^{\exp}(\mathrm{HFBz})}{A_{\nu_{6,10}}^{\exp}(\mathrm{HFBz})} \quad (7)$$

The population for the aryl-H conformer is

$$\beta = \frac{1 - \alpha}{1.62} \quad (8)$$

and for the D_{3h} conformer is

$$\chi = 0.62\beta \quad (9)$$

Details of the derivation as well as its relation to the analysis of the X-ray absorption spectra are depicted in Figure 2. The analysis of the PFBz spectra follows the same procedure. In that case, however, eq 3 is replaced by the relative population between the aryl-F and D_{3h} conformers. Its values have been calculated by fitting the temperature dependence of the measured normalized ν_1 peak areas of HFBz

$$\chi = 0.29\alpha \quad (3a)$$

To check the accuracy of the values, the populations have been also determined by a variation of our general method. We calculated the conformer populations of FBz using the measured normalized ν_1 peak areas of HFBz and also determined each conformer of PFBz using that of Bz. Both calculation procedures yielded similar results within ±10%. Based on the ratio of equilibrium conformer distribution from D_{3h} and non-D_{3h}, the Gibbs free energies for the IPC···S complexation have been calculated. All the conformer populations and their Gibbs free energies are listed in Table 2. The calculated conformer ratio of IPC in PFBz is in good agreement with its temperature-dependent experimental value.

All IR measurements followed the same procedures presented in ref 1. Briefly, $Fe(CO)_5$ was purchased from Aldrich (99.999%) and used as received. The solvents were purchased from Aldrich at 99%+ purity and used after static drying with 300-pm zeolite molecular sieves provided as beads with 4−8 mesh size.[66] All chemical preparation processes were carried out in a controlled atmosphere glovebox with on-line drying and oxygen trapping train under nitrogen atmosphere. The glovebox was illuminated with red-filtered light of low intensity to prevent any photochemical conversion. The IR absorption spectra were measured with a Mattson Infinity Golden FTIR spectrometer with sample solutions of either 0.01 M concentration and 50-μm sample

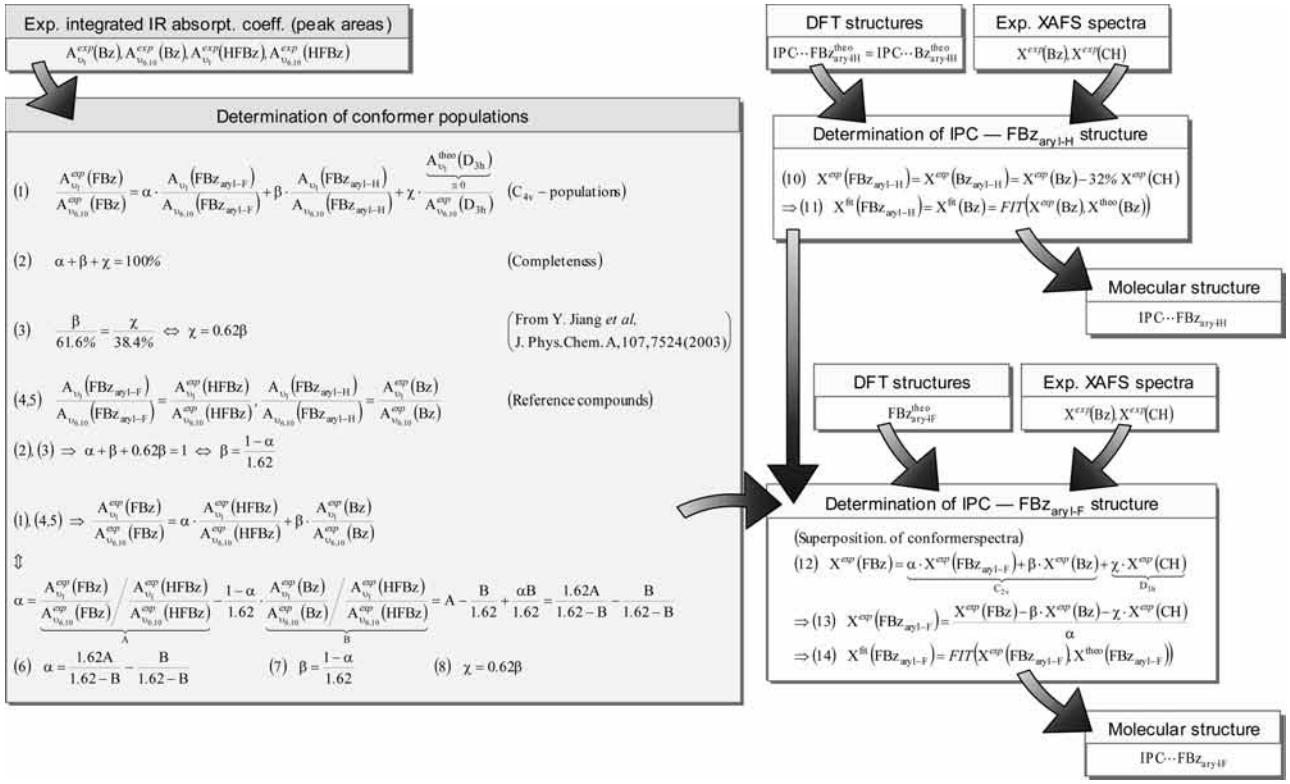

Figure 2. Scheme of concerted analysis procedure of infrared and X-ray absorption spectra.

TABLE 2: Summary of All Conformer Populations and Gibbs Free Energies for IPC Transitions from D_{3h} to C_{2v} Symmetry

Experimental Data

	D_{3h} [%]	non-D_{3h} [%]	ΔG_{conf} [kJ/mol]
CH[a]	100.0	0.0	
Bz[a]	38.4	61.6	−1.17
PFBz[a]	10.6	89.4	−5.29
HFBz[b]	22.6	77.4	−3.06

Calculated Data

	D_{3h} [%]	aryl-H [%]	aryl-F [%]	non-D_{3h} [%]	ΔG_{conf} [kJ/mol]
FBz	28.2	45.5	26.2	71.8	−2.31
PFBz	11.8	48.0	40.3	88.2	−5.00

[a] Reference 1, from temperature-dependent IR measurements. [b] This work, from temperature-dependent IR measurements.

thickness or 0.1 M concentration and 500-μm sample thickness sandwiched between two CaF_2 plates. Thus, the absorbance (optical density) of the solutions was varied by a factor of 100 with the lower absorbance being used for the measurements of the ν_6 and ν_{10} peaks. The larger concentration used for measurements of the ν_1 peak in the higher energy spectral range did not influence the shape of the measured spectra as checked by test measurements at 10 mM concentration, where the small peaks above 2100 cm^{-1} were well recognizable. Nevertheless, to improve the signal-to-noise ratio while maintaining the data acquisition time, the larger absorbance was chosen for this spectral range. The resolution of the FTIR spectrometer was 0.5 cm^{-1}. The spectra were fitted with Voigt profiles using the Origin Peak Fitting program. The data listed in Table 1 are the results of these fits. Initially, the ν_6 and ν_{10} peaks were fitted. Subsequently, we fitted the spectrum at 2100−2200 cm^{-1} using the wings of the ν_6 and ν_{10} peaks for background subtraction. Then, we used three Voigt profiles at the positions of $\nu_{10} + \nu_{18}$, ν_1, and $\nu_2 + \nu_{14}$; see Figure 6 in ref 1. These procedures were applied to the sample preparation for, and measurements of both, solvent-dependent and temperature-dependent FTIR spectra. Afterward, the ν_1 peak areas were analyzed and yielded the conformer populations.

3. Conformer Structures

The structures of the conformers were determined using XAFS measurements in combination with density functional theory (DFT) calculations. The conformer populations obtained above were used to separate the measured spectra into the spectral contributions of each conformer. XAFS relies on the ionization of an inner atomic shell electron by absorption of a single X-ray photon with an energy larger than the electron's ionization energy. As a consequence, the X-ray absorption cross section of an atom inside of a molecule, for example, the iron atom in $Fe(CO)_5$, increases suddenly. Modulations of the cross section as a function of increasing X-ray photon energy contain the desired structural information. Further details have been discussed extensively in the literature.[67,68] X-ray absorption spectra are typically considered in two parts: X-ray absorption near-edge structure (XANES) and extended X-ray absorption fine structure (EXAFS). XANES contains information about the density of valence states of the absorber, as well as structural information, which is often interpreted by simulation. EXAFS spectra are determined by single scattering events of electrons propagating between iron and the surrounding atoms. Thus, EXAFS spectra measure the first-order atomic pair correlation functions between iron and its surrounding atoms. Similar to the analysis of the IR spectra, the X-ray absorption spectra are superpositions of the XAFS spectra of the conformers. For instance, the measured XAFS of IPC in Bz is a superposition of 62% IPC···Bz and 38% D_{3h} conformer spectrum. The D_{3h} conformer spectrum is known from the measurement of the XAFS spectra of IPC in CH because the nearly complete absence of a ν_1 peak in the IR spectra proves that IPC in CH has retained its D_{3h} symmetry. Therefore, the XAFS spectrum

TABLE 3: Experimental and DFT-Calculated Structural Data of IPC···CH

	IPC−CH NSLS	IPC−D_{3h} DFT results (averaged)
R(Fe−C) [pm]	182.3 ± 0.2	180.9
R(Fe−O) [pm]	293.8 ± 0.2	295.9
R(C−O) [pm]	111.5 ± 0.24	114.9
σ^2(Fe−C) [pm^2]	19.6 ± 2.7	
σ^2(Fe−O) [pm^2]	12.4 ± 2.1	
S_0^2	0.878 ± 0.011	
E_0 [eV]	6.13 ± 0.10	
residual [%]	18.0	

TABLE 4: DFT-Calculated Structural Data of Various IPC···S Complexes with Aryl-H Interacting with IPC

	IPC−Bz	IPC−Bz	IPC−PFBz
R(Fe−C) [pm]	181.0	181.0	181.1
R(Fe−O) [pm]	295.9	295.9	296.0
R(C−O) [pm]	114.9	114.9	114.8
R(Fe−H) [pm]	250.0[a]	250.0[a]	250.0[a]

[a] Fixed distance during DFT calculations.

TABLE 5: DFT-Calculated Structural Data of Various IPC···S Complexes with Aryl-F Interacting with IPC

	IPC−FBz	IPC−PFBz	IPC−HFBz
R(Fe−C) [pm]	180.8	181.0	181.0
R(Fe−O) [pm]	295.9	296.0	296.0
R(C−O) [pm]	115.1	115.0	115.0
R(Fe−F) [pm]	260.0[a]	260.0[a]	260.0[a]

[a] Fixed distance during DFT calculations.

TABLE 6: Experimental Structural Data of Various IPC···S Complexes with Aryl-H Interacting with IPC

	IPC−Bz	IPC−FBz	IPC−PFBz
R(Fe−C) [pm]	181.9 ± 0.21	182.1 ± 0.19	181.6 ± 0.18
R(Fe−O) [pm]	292.6 ± 0.19	293.5 ± 0.17	293.0 ± 0.17
R(C−O) [pm]	110.7 ± 0.28	111.4 ± 0.26	111.3 ± 0.25
R(Fe−H) [pm]	246.7 ± 12.16	246.5 ± 12.08	245.3 ± 12.66
σ^2(Fe−C) [pm^2]	28.6 ± 3.21	21.6 ± 2.88	7.7 ± 2.39
σ^2(Fe−O) [pm^2]	22.3 ± 19.27	13.1 ± 2.22	7.5 ± 2.11
σ^2(Fe−H) [pm^2]	1.0 + 133.18	1.0 + 130.78	1.0 + 135.37
S_0^2	0.9 ± 0.01	0.8 ± 0.01	0.9 ± 0.01
E_0 [eV]	5.6 ± 0.14	5.6 ± 0.13	5.5 ± 0.13
residual [%]	19.5	17.7	19.5

of IPC measured in CH is used to subtract the D_{3h} conformer contribution from the benzene spectrum. In eq 10 the corrected IPC···Bz spectrum is equal to that of the aryl-H conformer of IPC in Bz. Furthermore, it was equated to that of the aryl-H conformer of IPC solvated in FBz.

$$X^{exp}(FBz_{aryl-H}) = X^{exp}(Bz_{aryl-H}) = X^{exp}(Bz) - 38\%X^{exp}(CH) \quad (10)$$

Subsequently, the IPC···FBz$_{aryl-H}$ spectrum was reproduced by a theoretical EXAFS spectrum calculated with FEFF 8.10. Our DFT-calculated structures of the aryl-H conformer with a hydrogen−iron distance of 250 pm were used as the starting structures for the structure refinement process. The best-fit X-ray spectrum is equal to the spectrum of Bz. Thus, the fitting process

$$X^{fit}(FBz_{aryl-H}) = X^{fit}(Bz) = FIT(X^{exp}(Bz),X^{theo}(Bz)) \quad (11)$$

yields the structural parameters of IPC(D_{3h}) and IPC···Bz$_{aryl-H}$. They are reproduced in Tables 3 and 6.

TABLE 7: Experimental Structural Data of Various IPC···S Complexes with Aryl-F Interacting with IPC

	IPC−FBz	IPC−PFBz	IPC−HFBz
R(Fe−C) [pm]	182.1 ± 0.32	181.4 ± 0.21	181.6 ± 0.19
R(Fe−O) [pm]	294.7 ± 0.23	293.1 ± 0.20	293.2 ± 0.20
R(C−O) [pm]	112.7 ± 0.39	111.7 ± 0.29	111.6 ± 0.27
R(Fe−F) [pm]	264.9 ± 3.07	253.6 ± 1.41	258.0 ± 1.90
σ^2(Fe−C) [pm^2]	1.0 + 2.83	1.0 + 2.73	1.0 + 2.51
σ^2(Fe−O) [pm^2]	1.0 + 2.82	1.0 + 2.49	2.9 ± 2.56
σ^2(Fe−F) [pm^2]	39.6 + 40.08	1.0 + 16.16	24.0 + 25.23
S_0^2	0.6 ± 0.01	0.7 ± 0.01	0.7 ± 0.01
E_0 [eV]	5.6 ± 0.14	5.6 ± 0.14	6.0 ± 0.13
residual [%]	27.8	21.4	18.3

The measured XAFS spectrum of IPC···FBz is a superposition of the C_{2v} and D_{3h} conformers:

$$X^{exp}(FBz) = \alpha X^{exp}(FBz_{aryl-F}) + \underset{C_{2v}}{\beta X^{exp}(Bz)} + \underset{D_{3h}}{\chi X^{exp}(CH)} \quad (12)$$

with the conformer populations α, β, and χ defined by eqs 6, 8, and 9. The experimental XAFS spectrum for IPC···FBz$_{aryl-F}$ can be obtained from eq 13.

$$X^{exp}(FBz_{aryl-F}) = \frac{X^{exp}(FBz) - \beta X^{exp}(Bz) - \chi X^{exp}(CH)}{\alpha} \quad (13)$$

This spectrum was fitted using the DFT-calculated structures of the aryl-F conformer with a fluorine−iron distance of 260 pm as the initial structure estimate as described by

$$X^{fit}(FBz_{aryl-F}) = FIT(X^{exp}(FBz_{aryl-F}),X^{theo}(FBz_{aryl-F})) \quad (14)$$

The resulting structural data are listed in Table 7. In general, we analyzed the EXAFS portion of the XAFS data by calculating theoretical spectra while fitting the scattering path lengths of the photoelectron until best agreement with the measured data was obtained. The initial scattering paths were calculated based on DFT structures of the IPC···S complexes listed in Tables 4 and 5. It is desirable that the EXAFS fitting process and the DFT structure calculations are combined in a closed-loop process, but such a procedure is currently too complicated. Furthermore, the nearest solvation shell should be included in the XAFS analysis. Nevertheless, the structures of other symmetric complexes, such as $Ni(CN)_4^{2-}$ and $Fe(CN)_6^{3-/4-}$, have been successfully analyzed without consideration of the solvation shells.[69,70] Here we ignore the solvation shells as well because the resulting structural fluctuations will randomize the phases of the electron scattering paths. As a consequence, their contributions to the XAFS spectrum cancel out. However, even without the solvation shell, considering only up to third-order scattering paths, about 60 single and multiple scattering paths exist within a radius of 4 Å around the iron atom. Not all of them can be included in the fitting process because the number of fit parameters would exceed the amount of structural information contained in the XAFS spectra. In general, this information increases with increasing spectral range over which X-ray absorption modulations are measured, which is why it is desirable to measure spectra over the largest possible X-ray

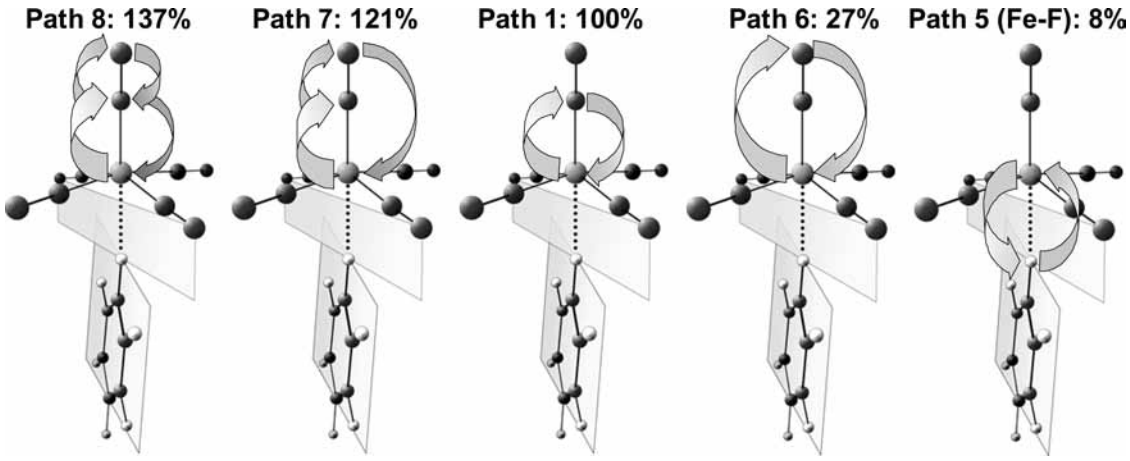

Figure 3. Photoelectron scattering paths used for structural fitting of XAFS spectrum.

energy range. Stern[71] derived that the number of independent points contained in an XAFS spectrum is

$$N_I = \frac{2\Delta k \Delta R}{\pi} + 2 \tag{15}$$

Here, Δk is the analyzed wavenumber range of the XAFS spectrum and ΔR is the range of the electron scattering path lengths over which the fit is made. In our case, $\Delta k = 10.5$ Å^{-1}, $\Delta R = 1.2$ Å, which yields $N_I = 10$. Thus a theoretical XAFS spectrum described by up to 10 parameters, such as atomic distances from the iron atom to surrounding atoms and their corresponding Debye−Waller factors, can be fitted to the data. Usually additional parameters have to be included. These parameters include the amplitude reduction factor, S_0^2, a correction E_0 to the theoretical ionization energy, and possible multiple scattering path lengths between ligands. Since IPC has 10 ligand atoms, a theoretical XAFS spectrum that explicitly includes all distances greatly exceeds N_I and a reduction of fit parameters is required. We therefore represent the individual scattering paths within each of the 10 ligand atoms by common paths while increasing the relative contributions of the new representative paths by a factor of 5. These paths are depicted in Figure 3. All other scattering paths were neglected either because their scattering amplitudes are small or because thermal vibrations of soft modes with large Debye−Waller factors effectively randomize the waves' phases such that their contributions cancel out. Furthermore, the remaining paths 7 and 8 are correlated with path 6, and a common distance R_6 and a Debye−Waller factor σ_6 can be used for their parametrization. Thus, the structural fits were carried out using the following eight independent parameters:

$$\begin{gathered}
\sigma^2(\text{Fe}-\text{O}) = {\sigma_6}^2 = {\sigma_7}^2 = {\sigma_8}^2 \\
R(\text{Fe}-\text{O}) = R_6 = R_7 = R_8 \\
\sigma^2(\text{Fe}-\text{C}) = {\sigma_1}^2 \\
R(\text{Fe}-\text{C}) = R_1 \\
\sigma^2(\text{Fe}-\text{H/F}) \\
R(\text{Fe}-\text{H/F}) \\
{S_0}^2, \qquad E_0
\end{gathered} \tag{16}$$

The coordination number of paths 1, 6, 7, and 8 remained fixed at 5 and that of path 5 for Fe−H/F was set to 1. The path labeled Fe−H/F refers to the single scattering path between iron and aryl hydrogen or aryl fluorine for the aryl-H and aryl-F conformers, respectively. The measured XAFS spectra of IPC solvated in benzene and its fluorinated derivatives are shown in Figure 4. The spectra were measured at the National Synchrotron Light Source, beam line X11B, which had a Si(111) channel-cut double crystal, with step sizes ranging from 0.25 to 1 eV for up to 200 eV above the iron K edge and 0.05 Å^{-1} step size in k-space for the higher energy region. Before further data analysis, all the data points of the visible glitches in the original spectra were removed and subsequently replaced with points obtained through polynomial interpolation. Data reduction of experimental absorption spectra and EXAFS fitting were carried out using WinXAS 3.1.[72] Background subtraction and normalization was carried out by fitting a polynomial to the preedge and postedge regions of an absorption spectrum. A smooth atomic background, $\mu_0(k)$, was obtained using cubic splines. Using FEFF 8.10,[73−75] the EXAFS sections of the spectra were analyzed through multiple scattering fitting using the parameters from eq 16. Table 6 shows the fitted structural parameters of IPC···Bz_{aryl-H}, IPC···FBz_{aryl-H}, and IPC···$PFBz_{aryl-H}$. Table 7 shows the fitted structural parameters of IPC···FBz_{aryl-F}, IPC···$PFBz_{aryl-F}$, and IPC···$HFBz_{aryl-F}$. As an illustration of the quality of the fitting process, the experimental XAFS spectrum of IPC···$HFBz_{aryl-F}$ and the fitted spectrum are shown in Figure 5. The k^2-weighted experimental and the fitted XAFS spectra were Fourier transformed using identical parameters. The resulting radial distribution functions are both compared in Figure 6. The transformations were carried out without any phase correction of the scattering electron waves and, consequently, the absolute values of the abscissa are downshifted. The peak position agreement of better than 1 pm confirms the numerical precision for the fitted iron−ligand atom distances listed in Tables 6 and 7.

The scattering amplitude of the Fe−H path is very small, and we therefore do not believe that our measurements permit a reliable measurement of the Fe−H distance. In addition, the small σ^2 values for the Fe−H paths result from very low electron density for that scattering path. This is numerically expressed in the large uncertainty for this distance and σ^2 value in Table 6. In contrast, the Fe−F distances are much more reliable, as shown in Table 7. This was confirmed by test calculations that did not include the Fe−F scattering path. Removing the fluorine atom and then optimizing the EXAFS fit yields a residual of 20.0% in contrast to the residual of 18.2% for a fit that includes the Fe−F path. Thus, while the difference is not large, the fluorine atom noticeably contributes to the fit. The small σ^2

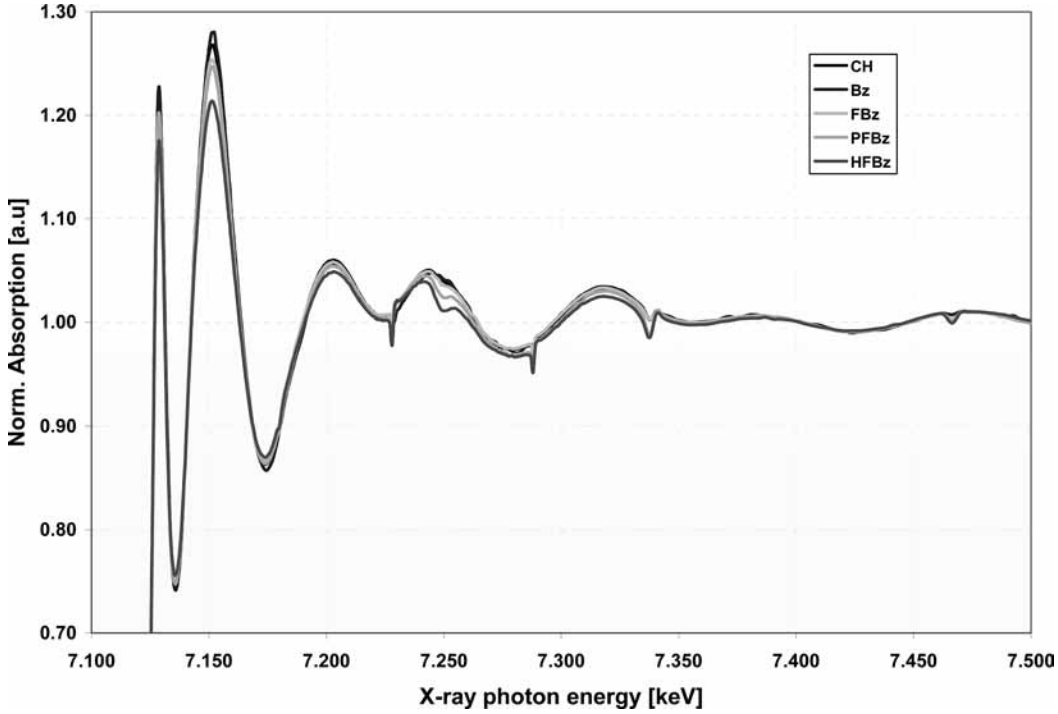

Figure 4. Experimental XAFS spectra of IPC in various solvents.

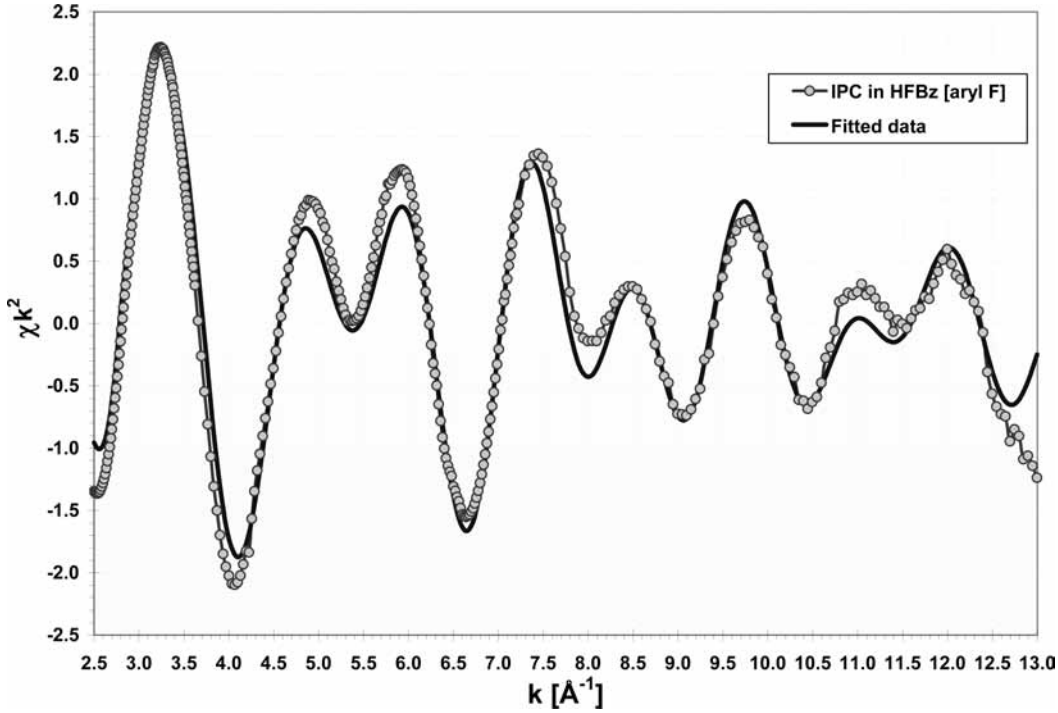

Figure 5. Comparison of experimental XAFS spectrum of HFBz and spectrum of the best structural fit.

values for Fe−C and Fe−O paths in IPC−S_{aryl-F} are caused by noise at higher k values. This was verified by reducing the k_{max} value during fitting by 1 Å^{-1}. Consequently, the residuals were improved by 1−2% and some of the σ^2 values increased by a few square picometers.

4. Discussion

Solvation of IPC generally causes a red shift of the CO stretching vibration frequencies, and the peak positions of the CO stretching vibrations in Bz are blue shifted relative to those in CH. Increasing fluorination of benzene, however, blue shifts the peak positions relative to Bz. This is caused by a reduction of electron density in the π back-bonding orbitals within IPC, which, in turn, causes an increase in the iron−ligand distances and a simultaneous decrease in the carbonyl bond lengths and an increase of bond strength. The DFT-calculated structural data show that increasing fluorination of benzene induces an increasing deformation of IPC toward C_{4v} symmetry. As a consequence, the CO−Fe−CO angle of the axial ligands decreases and the angle between the equatorial ligands in the plane of the solvent attack increases. This effect occurs for both the aryl-H and the aryl-F conformer complexes as shown in Figure 7. The angles for the aryl-H complexes were calculated at 250 pm IPC···S distance. While the angles of the aryl-F complexes were

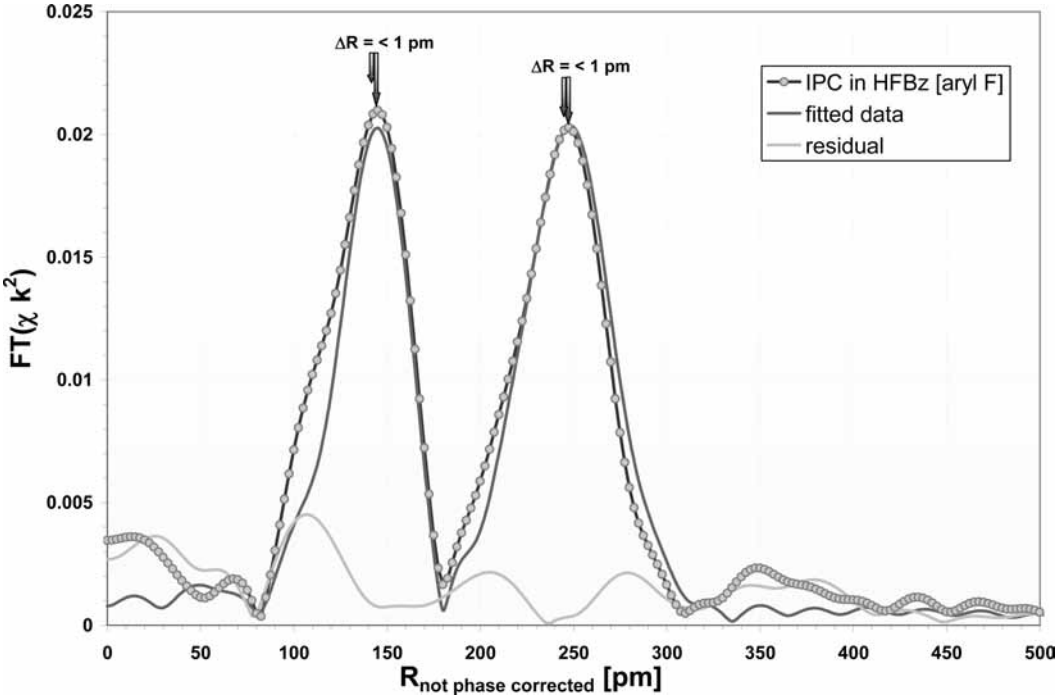

Figure 6. Radial distribution function of experimental XAFS spectrum of HFBz and that of the best structural fit.

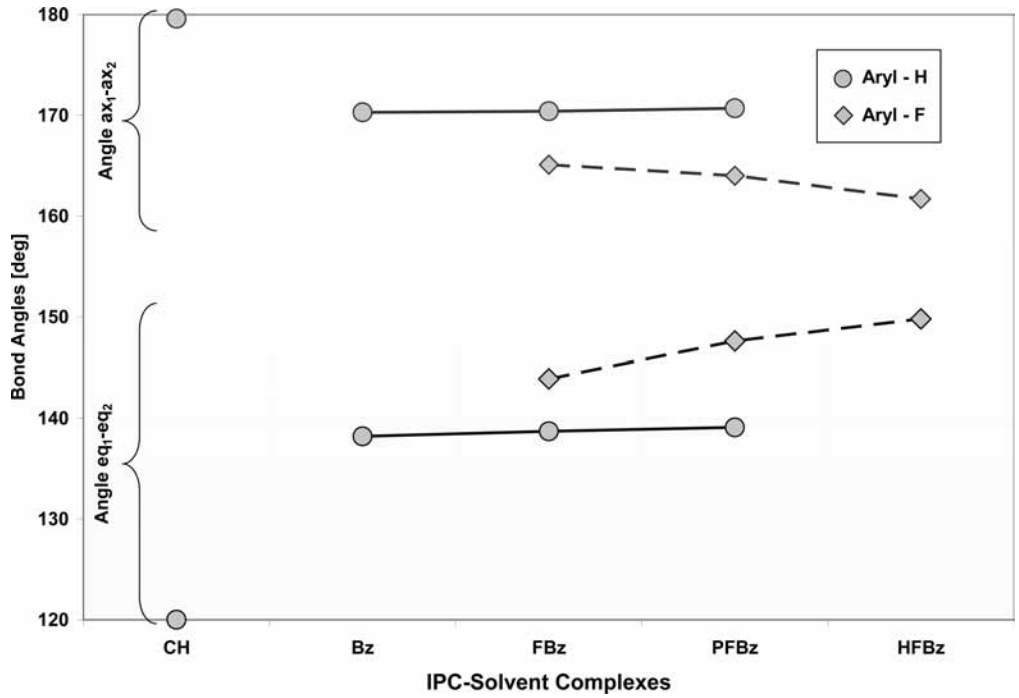

Figure 7. Theoretical ligand−Fe−ligand bond angles for the aryl-H and aryl-F conformers of Bz, FBz, PFBz, and HFBz. The aryl-H conformer structural data were calculated for an IPC···S distance of 250 pm; the aryl-F conformer structural data were calculated for an IPC···S distance of 260 pm. The bond angle labels correspond to the ligand labels in Figure 1. For reference, the corresponding angles for undistorted IPC in cyclohexane are shown.

calculated at a 10 pm larger distance, the induced deformations are more pronounced. These deformations are accompanied by an electron density shift from IPC toward the complexated solvents. Such shifts cause a reduction of electron density in the π back-bonding orbitals within IPC. This increases the C−O bond strengths, which, in turn, blue shifts the IR peaks. We observed this theoretically predicted shift as shown in Table 1. Furthermore, the ratio of the $M_1/(M_2 + M_3)$ peak areas, corresponding to the ratio ν_{10}/ν_6 for D_{3h} symmetry, decreases from CH to Bz and further with increasing fluorination. For HFBz, however, this ratio increases again. This trend indicated an increasing deformation of IPC from D_{3h} toward C_{4v}. Jiang et al.[1] showed in their Table 1 that the peak ratio initially decreases for increasingly deformed IPC but eventually increases above the value for D_{3h} as a C_{4v} symmetry is approached. Thus, the IR data support the theoretically predicted deformation.

The symmetry changes are accompanied by a slight bond length reduction within IPC with increasing benzene fluorination and aryl-F interaction as shown in Table 7. Simultaneously, the distance between Fe and aryl-F decreases by about 11 pm going from FBz to PFBz, but it increases again for the IPC···HFBz complex. This implies that the interaction between IPC and

PFBz is stronger than the interaction between IPC and HFBz, which, in turn, implies that the non-D_{3h} population of IPC in PFBz is larger than the one in HFBz. Thus, the XAFS data and the FTIR data are in general agreement with each other and follow the trend suggested by the DFT calculations.

The population calculations introduced in section 2 are based on the assumption that the IR peak areas of IPC interacting with aryl-F and aryl-H, respectively, are identical for all solvents. This ignores the fact that the deformation of IPC increases with increasing solvent fluorination, as shown in Figure 7. For instance, eq 4 is not entirely accurate because the interaction with the aryl-F of HFBz induces a larger deformation of IPC than the interaction with aryl-F of FBz. As a consequence, Table 1 of ref 1 suggests that the relative ν_1 peak area should be larger in HFBz than in FBz. Thus, in principle, the recovery of the conformer populations depends on the knowledge of the IPC···S structures, which can only be calculated after the iron−fluorine distances have been measured by XAFS. The analysis of the XAFS spectra, however, depends on the knowledge of the conformer populations. This implies that an iterative process that includes the IR analysis, XAFS analysis, and DFT calculations might be needed. While this is in principle true, we estimated that the errors caused by the assumption made in eqs 4 and 5 are a few percent. For instance, the precision of the population recovery process can be estimated by a 10% variation of the relative ν_1 peak area of IPC−FBz in eqs 4 and 5. This causes a decrease of the calculated aryl-H conformer population from 45.5% to 42.6%. Simultaneously, the aryl-F population increases from 26.2% to 31.1% and the D_{3h} conformer population decreases from 28.2% to 26.4%. Thus, the overall error is smaller than 5% for a 10% uncertainty of the ν_1 peak area.

One of the goals of this study is the determination of the equilibrium structures of solvated IPC for later use as initial structures in ultrafast laser-pump XAFS-probe measurements using laser plasma X-ray sources. The first of such measurements have recently been performed.[76] The ultrafast atomic motions during photoinduced ligand substitution reaction depend on the equilibrium structure before photoexcitation. We have shown that complexing solvents induce substantial deformations of IPC while noncomplexing solvents do not. Here we define a solvent as complexing if more than 50% of all IPC molecules form an IPC···S complex at room temperature. Thus, we consider Bz and its fluorinated derivatives a complexing solvent and CH a noncomplexing solvent. Most likely other alkanes are noncomplexing as well.

The interaction strength of Bz increases with increasing fluorination as indicated by the increasing blue shift of the IR peaks, the increasing structural deformation of IPC, and the reduced Fe−solvent distance. As a consequence, ligand substitution reactions do not have to proceed through a dissociative process. Instead, a concerted process might occur with one carbonyl leaving as the solvent forms a chemical bond. Based in part on time-resolved optical pump−probe data from ref 16, Scheme 1 depicts possible reaction mechanisms for complexing and noncomplexing solvents. For noncomplexing solvents, the reaction dynamics in the first picoseconds are likely to be similar to the gas-phase dynamics. Ultrafast gas-phase dissociation studies have demonstrated that the UV photolysis of IPC causes the loss of a single CO ligand within 150 fs via a conical intersection.[16] The ligand dissociation likely proceeds via pseudorotation during the relaxation from ^{1}[Fe(CO)$_4$]* to ^{1}Fe(CO)$_4$,[16−18,77] corresponding to (^{1}**2***) and (^{1}**2**), respectively. The vibrationally hot ^{1}[Fe(CO)$_4$]* may lose further ligands within several picoseconds.[16−18] This rapid dissociation process

SCHEME 1 [a]

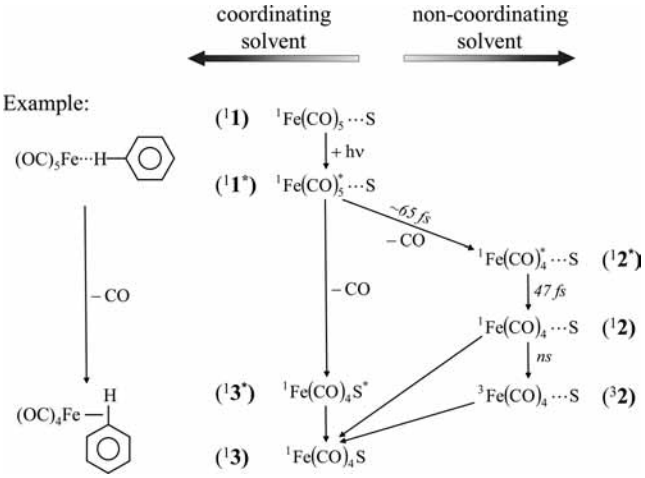

[a] Left: suggested ligand substitution mechanism in complexing solvents. Right: possible reaction mechanism in noncomplexing solvents. The reaction times are taken from ref 16.

makes the involvement of a triplet intermediate highly unlikely, and multiple ligands can be lost without any intersystem crossing. Of course, in solution excess energy is quickly dissipated into the solvent and multiple ligand loss does not occur as observed in the literature.[14,78,79] Subsequently, with relaxation on the nanosecond time scale, the electronic ground state ^{3}Fe(CO)$_4$, (^{3}**2**), and finally the substituted product (^{1}**3**) can be reached. Thus, if Fe(CO)$_4$ is formed during the reaction, two intersystem crossings (ISC) have to occur in order to reach the product (^{1}**3**). Alternatively, intersystem crossing might occur within IPC after photoexcitation but before CO dissociation.[80] Such a triplet state would, in principle, directly correlate with (^{3}**2**). However, based on the measured times of less than 100 fs[16] for the reaction from (^{1}**1***) to (^{1}**2**), such early intersystem crossings can be excluded. Snee et al.[20] observed the formation of ^{3}Fe(CO)$_4$, (^{3}**2**), in dry heptane after about 26 ps using time-resolved infrared spectroscopy. (^{3}**2**) was identified by its close similarity to the expected triplet IR spectra. It existed for at least 660 ps without apparent substitution product formation, showing that the reaction from (^{3}**2**) to (^{1}**3**) is very slow in noncomplexing solvents. As discussed above, we consider ISC within Fe(CO)$_5$ unlikely. Consequently, the production of (^{3}**2**) requires the formation of (^{1}**2**), which has not been observed. It might be possible that the IPC−solvent interaction accelerates ISC from (^{1}**2**) to (^{3}**2**), but this seems unlikely in a noncoordinating solvent. Furthermore, it does not explain why the reaction would not proceed from (^{1}**2**) directly to (^{1}**3**), since the reaction between singlet complexes and alkanes should be fast. This situation is somewhat puzzling.

In contrast, the left side of Scheme 1 depicts our suggestion for a concerted substitution mechanism in complexing solvents. This path does not involve any intersystem crossing. We suggest that (^{1}**1**) after photoexcitation in complexing solvents proceeds directly from (^{1}**1***) to (^{1}**3***) and (^{1}**3**). No triplet intermediate is formed, and the reaction rate is not limited by the diffusive encounter between IPC and S. As an example, the product IPC−Bz is shown. The molecular structure is not known and the product is not long-term stable. However, it has been identified by Church et al.[81] after photodissociation of Fe(CO)$_5$ solvated in benzene. Their 5-μs temporal resolution was too long to permit the measurement of the rate constant for the reaction step of (^{1}**1***) to (^{1}**3**). Its IR spectrum is similar to that of Fe(CO)$_4$(η^2-alkene) complexes, which suggests that benzene is also bound in η^2-coordination.[81,82]

While we believe that our and other authors' evidence supports the distinction of separate reaction mechanisms for complexing and noncomplexing solvents, details of the molecular dynamics and the reaction mechanisms remain unclear. More information might be obtainable through time-resolved structural measurements. Ultrafast structural measurements of the IPC dissociation reaction have been carried out in the gas phase.[17] We recently succeeded in measuring the first laser-pump ultrafast XAFS-probe signal of solvated iron hexacyanide using our laser plasma X-ray source.[76] Ultrafast XAFS measurements of the photosubstitution reaction in complexing and noncomplexing solvents will likely provide the opportunity to distinguish between the reaction mechanisms shown in Scheme 1.[83] For instance, Snee et al.[20] calculated that the Fe−CO-ligand bond lengths in (^{3}**2**) are approximately 6 pm longer than that in (^{1}**2**). Singlet product distances are shorter again. Such distance changes would noticeably shift the XAFS spectrum, thereby permitting the identification of the triplet intermediate. In contrast, the singlet reaction mechanism would be characterized by a rather constant bond length. Furthermore, the suggested agostic interaction between IPC and benzene, shown in Scheme 1, would cause substantial changes in the XANES spectrum as shown by Lee et al.[83]

5. Conclusion

The equilibrium structures of IPC solvated in benzene and its fluorinated derivatives have been measured by FTIR and XAFS spectroscopies. DFT structures were used as input for the XAFS analysis. It was found that IPC forms complexes with a single solvent molecule. The interaction strength increases with increasing fluorination of the solvent. In an extension of our previous work using only IR spectroscopy, the IPC−solvent distances could be measured for several of the simultaneously present conformers.

The complexation between IPC and coordinating solvents makes concerted ligand substitution processes very likely. This, in turn, should suppress any theoretically possible reaction mechanisms that involve triplet intermediates. These properties should be prototypical for a larger class of monometallic systems, which are electronically saturated but not sterically crowded. These IPC−S complexes offer important opportunities for UXAFS investigations of the ultrafast dynamics of bimolecular reactions because the photoinduced bimolecular reactions may preserve vibrational coherence from the reactants, observed in the gas phase for various transition metal carbonyls,[77,84] to the products.

Acknowledgment. The authors gratefully acknowledge partial funding and support for this work by the National Science Foundation, Grant CHE-9984890, and the Research Corporation, Grant RI0455. This research was carried out in part at the National Synchrotron Light Source, Brookhaven National Laboratory, which is supported by the U.S. Department of Energy, Division of Materials Sciences and Division of Chemical Sciences, under Contract No. DE-AC02-98CH10886. The authors thank Dr. Peter Siddons for help during the measurements at NSLS.

References and Notes

(1) Jiang, Y.; Lee, T.; Rose-Petruck, C. *J. Phys. Chem. A* **2003**, *107*, 7524−7538.
(2) Hoye, T. R.; Suriano, J. A. *J. Am. Chem. Soc.* **1993**, *115*, 1154−1156.
(3) Cheng, H.; Reiser, D. B.; Dean, S. W., Jr.; Baumert, K. *J. Phys. Chem. B* **2001**, *105*, 12547−12552.
(4) Knolker, H.-J. *Chem. Soc. Rev.* **1999**, *28*, 151−157.
(5) Suslick, K. S.; Hyeon, T.; Fang, M.; Cichowlas, A. A. *Adv. Catal. Nanostruct. Mater.* **1996**, 197−212.
(6) Wrighton, M. *Chem. Rev. (Washington, D.C.)* **1974**, *74*, 401−430.
(7) Geoffroy, G. L.; Wrighton, M. S. *Organometallic photochemistry*; Academic Press: New York, 1979.
(8) Bañares, L.; Baumert, T.; Bergt, M.; Kiefer, B.; Gerber, G. *J. Chem. Phys.* **1998**, *108*, 5799−5811.
(9) Bañares, L.; Baumert, T.; Bergt, M.; Kiefer, B.; Gerber, G. *Chem. Phys. Lett.* **1997**, *267*, 141−148.
(10) Heilweil, E. J.; Cavanagh, R. R.; Stephenson, J. C. *J. Chem. Phys.* **1988**, *89*, 230−239.
(11) Lorono, M.; Cruse, H. A.; Davies, P. B. *J. Mol. Struct.* **2000**, *519*, 199−204.
(12) Asselin, P.; Soulard, P.; Tarrago, G.; Lacome, N.; Manceron, L. *J. Chem. Phys.* **1996**, *104*, 4427−4433.
(13) Lian, T.; Yang, H.; Asplund, M.; Bromberg, S. E.; Harris, C. B. Femtosecond IR studies of solvation by probing the solvent. In *Springer Series in Chemical Physics*; Toennies, J. P., Ed., Springer: New York, 1996; Vol. 62, pp 300−301.
(14) Joly, A. G.; Nelson, K. A. *Chem. Phys.* **1991**, *152*, 69−82.
(15) King, J. C.; Zhang, J. Z.; Schwartz, B. J.; Harris, C. B. *J. Chem. Phys.* **1993**, *99*, 7595−7601.
(16) Trushin, S. A.; Fuss, W.; Kompa, K. L.; Schmid, W. E. *J. Phys. Chem. A* **2000**, *104*, 1997−2006.
(17) Ihee, H.; Cao, J.; Zewail, A. H. *Angew. Chem., Int. Ed.* **2001**, *40*, 1532−1536.
(18) Poliakoff, M.; Turner, J. J. *Angew. Chem., Int. Ed.* **2001**, *40*, 2809−2812.
(19) Snee, P. T.; Payne, C. K.; Mebane, S. D.; Kotz, K. T.; Harris, C. B. *J. Am. Chem. Soc.* **2001**, *123*, 6909−6915.
(20) Snee, P. T.; Payne, C. K.; Kotz, K. T.; Yang, H.; Harris, C. B. *J. Am. Chem. Soc.* **2001**, *123*, 2255−2264.
(21) Yang, H.; Snee, P. T.; Kotz, K. T.; Payne, C. K.; Frei, H.; Harris, C. B. *J. Am. Chem. Soc.* **1999**, *121*, 9227−9228.
(22) Kotz, K. T.; Yang, H.; Snee, P. T.; Payne, C. K.; Harris, C. B. Ultrafast infrared studies of ligand rearrangement at coordinatively unsaturated transition metal centers. In *Springer Series in Chemical Physics*; Springer: New York, 2001; Vol. 66, pp 636−638.
(23) Kotz, K. T.; Yang, H.; Snee, P. T.; Payne, C. K.; Harris, C. B. *J. Organomet. Chem.* **2000**, *596*, 183−192.
(24) Fuss, W.; Trushin, S. A.; Schmid, W. E. *Res. Chem. Intermed.* **2001**, *27*, 447−457.
(25) Demuynck, J.; Strich, A.; Veillard, A. *Nouv. J. Chim.* **1977**, *1*, 217−228.
(26) Rossi, A. R.; Hoffmann, R. *Inorg. Chem.* **1975**, *14*, 365−374.
(27) Braga, D.; Grepioni, F.; Orpen, A. G. *Organometallics* **1993**, *12*, 1481−1483.
(28) Beagley, B.; Cruickshank, D. W. J.; Pinder, P. M.; Robiette, A. G.; Sheldrick, G. M. *Acta Crystallogr., Sect. B* **1969**, *B25*, 737−744.
(29) Beagley, B.; Schmidling, D. G. *J. Mol. Struct.* **1974**, *22*, 466−468.
(30) Braga, D.; Grepioni, F.; Orpen, A. G. *Organometallics* **1994**, *13*, 3544−3556.
(31) Berry, R. S. *J. Chem. Phys.* **1960**, *32*, 933−938.
(32) Blyholder, G.; Springs, J. *Inorg. Chem.* **1985**, *24*, 224−227.
(33) Jang, J. H.; Lee, J. G.; Lee, H.; Xie, Y.; Schaefer, H. F., III *J. Phys. Chem. A* **1998**, *102*, 5298−5304.
(34) Spiess, H. W.; Grosescu, R.; Haeberlen, U. *Chem. Phys.* **1974**, *6*, 226−234.
(35) Cotton, F. A.; Dunne, T. G.; Wood, J. S. *Inorg. Chem.* **1965**, *4*, 318−325.
(36) Raymond, K. N.; Corfield, P. W. R.; Ibers, J. A. *Inorg. Chem.* **1968**, *7*, 1362−1372.
(37) Spiro, T. G.; Terzis, A.; Raymond, K. N. *Inorg. Chem.* **1970**, *9*, 2415−2420.
(38) Riedel, E. F.; Jacobson, R. A. *Inorg. Chim. Acta* **1970**, *4*, 407−411.
(39) Cramer, R. D.; Lindsey, R. V., Jr.; Prewitt, C. T.; Stolberg, U. G. *J. Am. Chem. Soc.* **1965**, *87*, 658.
(40) Apostolova, E. S.; Tikhonov, A. P.; Sendyurev, O. A. *Russ. J. Coord. Chem.* **2002**, *28*, 38−45.
(41) Tanabe, T.; Morisato, T.; Suzuki, Y.; Matsumoto, Y.; Wadayama, T.; Hatta, A. *Vibr. Spectrosc.* **1998**, *18*, 141−147.
(42) Zaera, F. *Surf. Sci.* **1991**, *255*, 280−288.
(43) Poiarkova, A. V.; Rehr, J. J. *Phys. Rev. B: Condens. Matter* **1999**, *59*, 948−957.
(44) Poiarkova, A. V.; Rehr, J. J. *J. Synchrotron Radiat.* **1999**, *6*, 313−314.
(45) Van Hung, N.; Rehr, J. J. *Phys. Rev. B: Condens. Matter* **1997**, *56*, 43−46.
(46) *Jaguar 5.5*; Schrodinger, Inc.: Portland, OR, 1991−2003.
(47) Jonas, V.; Thiel, W. *J. Chem. Phys.* **1995**, *102*, 8474−8484.

(48) Gutmann, V. *Monatsh. Chem.* **1977**, *108*, 429−435.
(49) Bor, G. *Inorg. Chim. Acta* **1969**, *3*, 191−195.
(50) Bor, G. *Inorg. Chim. Acta* **1969**, *3*, 196−200.
(51) Bor, G.; Jung, G. *Inorg. Chim. Acta* **1969**, *3*, 69−73.
(52) Bor, G.; Sbrignadello, G.; Marcati, F. *J. Organomet. Chem.* **1972**, *46*, 357−368.
(53) McClelland, B. W.; Robiette, A. G.; Hedberg, L.; Hedberg, K. *Inorg. Chem.* **2001**, *40*, 1358−1362.
(54) Edgell, W. F.; Dunkle, M. P. *J. Phys. Chem.* **1964**, *68*, 452−456.
(55) Bigorgne, M. *J. Organomet. Chem.* **1970**, *24*, 211−229.
(56) Cataliotti, R.; Foffani, A.; Marchetti, L. *Inorg. Chem.* **1971**, *10*, 1594−1597.
(57) Jones, L. H.; McDowell, R. S.; Goldblatt, M.; Swanson, B. I. *J. Chem. Phys.* **1972**, *57*, 2050.
(58) Haas, H.; Sheline, R. K. *J. Chem. Phys.* **1967**, *47*, 2996−3022.
(59) Edgell, W. F.; Wilson, W. E.; Summitt, R. *Spectrochim. Acta* **1963**, *19*, 863−872.
(60) Swanson, B. I.; Jones, L. H.; Ryan, R. R. *J. Mol. Spectrosc.* **1973**, *45*, 324−325.
(61) Jones, L. H.; McDowell, R. S. *Spectrochim. Acta* **1964**, *20*, 248.
(62) Cotton, F. A.; Kraihanzel, C. S. *Inorg. Chem.* **1963**, *2*, 533.
(63) El-Sayed, M. A.; Kaesz, H. D. *J. Mol. Spectrosc.* **1962**, *9*, 310.
(64) Farona, M. F.; Cutcliffe, A. B. *Spectrosc. Lett.* **1970**, *3*, 89−92.
(65) Adams, D. M. *Metal-Ligand and Related Vibrations: a critical survey of the Infrared and Raman spectra of metallic and organometallic compounds*; Edward Arnold Ltd.: London, 1967.
(66) Reichardt, C. *Solvents and Solvent Effects in Organic Chemisrty*, 2nd ed.; VCH: New York, 1990.
(67) Agarwal, B. K. *X-ray Spectroscopy*, 2nd ed.; Springer-Verlag: Berlin, 1991; Vol. 15.
(68) *X-Ray Absorption—Principles, Applications, Techniques of EXAFS, SEXAFS, and XANES*; Koningsberger, D. C., Prins, R., Eds.; John Wiley & Sons: New York, 1988; Vol. 92.
(69) Munoz-Paez, A.; Diaz-Moreno, S.; Marcos, E. S.; Rehr, J. J. *Inorg. Chem.* **2000**, *39*, 3784−3790.
(70) Lee, T.; Benesch, F.; Jiang, Y.; Rose-Petruck, C. *Chem. Phys.* **2004**, *299*, 233−245.
(71) Stern, E. A. *Phys. Rev. B: Condens. Matter Mater. Phys.* **1993**, *48*, 9825−9827.
(72) Ressler, T. *J. Synchrotron Radiat.* **1998**, *5*, 118.
(73) Ankudinov, A. L.; Ravel, B.; Rehr, J. J.; Conradson, S. D. *Phys. Rev. B: Condens. Matter* **1998**, *58*, 7565−7576.
(74) Rehr, J. J.; Albers, R. C. *Rev. Mod. Phys.* **2000**, *72*, 621−654.
(75) Rehr, J. J.; Albers, R. C. *Phys. Rev. B: Condens. Matter* **1990**, *41*, 8139−8149.
(76) Lee, T.; Benesch, F.; Jiang, Y.; Rose-Petruck, C. Submitted for publication in *J. Chem. Phys.* **2004**.
(77) Trushin, S. A.; Fuss, W.; Schmid, W. E. *Chem. Phys.* **2000**, *259*, 313−330.
(78) Lian, T.; Bromberg, S. E.; Asplund, M.; Yang, H.; Harris, C. B. *J. Phys. Chem.* **1996**, *100*, 11994−12001.
(79) Joly, A. G.; Nelson, K. A. *J. Phys. Chem.* **1989**, *93*, 2876−2878.
(80) Daniel, C.; Benard, M.; Dedieu, A.; Wiest, R.; Veillard, A. *J. Phys. Chem.* **1984**, *88*, 4805−11.
(81) Church, S. P.; Grevels, F. W.; Hermann, H.; Kelly, J. M.; Klotzbuecher, W. E.; Schaffner, K. *J. Chem. Soc., Chem. Commun.* **1985**, 594−596.
(82) Leadbeater, N. *Coord. Chem. Rev.* **1999**, *188*, 35−70.
(83) *Ultrafast laboratory-based x-ray sources and their applications in chemical research*; Lee, T., Jiang, Y., Benesch, F., Rose-Petruck, C., Eds.; SPIE Publishing: Bellingham, WA, San Jose, CA, 2003; Vol. 4978, pp 77−91.
(84) Trushin, S. A.; Fuss, W.; Schmid, W. E.; Kompa, K. L. *J. Phys. Chem. A* **1998**, *102*, 4129−4137.